FEEL

Fast, Energy-Efficient Localization for Autonomous Indoor Vehicles

Gokhale, Vineet; Moyers Barrera, Gerardo ; Venkatesha Prasad, R.

DOI
10.1109/ICC42927.2021.9500500

Publication date
2021

Document Version
Accepted author manuscript

Published in
ICC 2021 - IEEE International Conference on Communications, Proceedings

FEEL: Fast, Energy-Efficient Localization for Autonomous Indoor Vehicles

Vineet Gokhale, Gerardo Moyers Barrera, R. Venkatesha Prasad
Embedded and Networked Systems, Delft University of Technology, The Netherlands

***Abstract*—Autonomous vehicles have created a sensation in both indoor and outdoor applications. The famous indoor use-case is process automation inside a warehouse using Autonomous Indoor Vehicles (AIV). These vehicles need to locate themselves not only with an accuracy of a few centimeters but also within a few milliseconds in an energy-efficient manner. Due to these challenges, *localization* is a holy grail. In this paper, we propose *FEEL* – an indoor localization system that uses a fusion of three low-energy sensors: IMU, UWB, and radar. We provide detailed software and hardware architecture of FEEL. Further, we propose *Adaptive Sensing Algorithm* (ASA) for optimizing for localization accuracy and energy consumption of FEEL by adjusting the sensing rate to the dynamics of the physical environment in real-time. Our extensive performance evaluation over diverse test settings reveals that FEEL provides a localization accuracy of sub-7 cm with an ultra-low latency of around 3 ms. Additionally, ASA yields up to 20% energy savings with only a marginal trade off in accuracy. Furthermore, we show that FEEL outperforms state of the art in indoor localization.**

***Index Terms*—Localization, FEEL, accuracy, energy-efficiency, latency, AIV**

I. Introduction

In this paper, we propose *FEEL* – a fast, accurate, and energy-efficient localization system using a sensor fusion of IMU, UWB, and radar for Autonomous Indoor Vehicles (AIV).

Recently, there have been many innovations and automation around the IoT, CPS, Industry 4.0, autonomous vehicles and drones. These innovations are paving ways for a few hundreds or thousands of AIV to collaboratively execute complicated industrial processes. As an example, several AIVs could be executing all tasks starting from supplying raw materials in a manufacturing process to stocking finished products in a warehouse. Efficiently performing these diverse tasks necessitate that the AIVs be capable of accurately sensing the operating environment in order to take intelligent decisions. A crucial part of this is *localization* – which is a *holy grail* – by which the AIVs learn their positions in the physical environment. In a dense environment with several obstacles and narrow paths, localization accuracy of 10 cm or lower is desired for safe operations. Furthermore, this should be achieved in a fast and an energy-efficient manner.

Why fast and energy-efficient? Several applications of (semi-)autonomous robots requiring ultra-low latency (<10 ms) are fast-emerging. Primary examples are the ones including fast control loops such as Tactile Internet [1] and FPV/autonomous drone racing [2]. Violation of latency requirements pose catastrophic consequences, such as crashes. This latency budget subsumes several processes like sensing, localization, path planning, communication, and actuation. In order to facilitate such applications with fast control loops, permissible localization latency is within a couple of milliseconds. In general, accurate and fast indoor localization can be achieved by employing powerful sensing (like LiDAR) and computational infrastructure. However, this is not always an affordable solution since the AIVs house small microcontrollers and are powered by batteries with limited energy budget in order to maintain a small form factor. Sub-optimal usage of energy results in frequent recharging and replacement of batteries, thereby contributing heavily towards the overall carbon footprint. Hence, achieving fast and energy-efficient localization while meeting the necessary accuracy requirement is a challenging research problem.

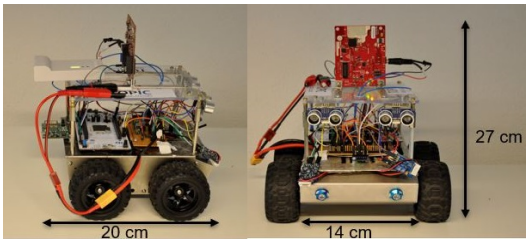

Fig. 1: Side and frontal views of *FEEL* – the proposed fast, energy-efficient, and accurate localization system for AIV.

For outdoor environments, Global Navigation Satellite System (GNSS) is the *de facto* localization method [3]. However, due to its poor localization accuracy in indoor environments, several other sensors have been extensively investigated. While vision-based sensors, like LiDAR and camera, can guarantee the required high accuracy for indoor environments, they are energy-intensive (sensing and computation) as well as unreliable under poorly illuminated conditions. Hence, other low-energy sensors, such as radar, Inertial Measurement Unit (IMU), odometry, Ultra-wideband (UWB), and WiFi have been extensively investigated in literature. Further, sensor fusion techniques are used to reap the benefits of simultaneously learning from multiple sensors.

Literature provides several combinations of the aforementioned low-energy sensors fused in a variety of ways to maximize the localization accuracy. However, to the best of our knowledge, none of these combinations yields the necessary

The first and last authors would like to thank Cognizant Technology Solutions and Rijksdienst voor Ondernemend Nederland under PPS O&I for sponsoring this research work under *Internet of Touch* project.

localization accuracy of sub-10 cm. Further, characterization of latency and energy efficiency of these localization methods have garnered negligible emphasis. In this work, we attempt to bridge this gap. Our contributions are summarized as follows.

- We present the design of *FEEL* – a system that fuses three low-energy sensors – IMU, UWB, and radar, for achieving fast and energy-efficient localization in the scale of a few centimeters in indoor environments. We design and develop a custom AIV (see Figure 1) for demonstrating the proof of concept of FEEL.
- We propose *Adaptive Sensing Algorithm* (ASA) for opportunistically minimizing the energy consumption of FEEL while marginally trading off accuracy by adjusting the sensing rate to suit the dynamics of the operation environment. ASA offers the flexibility to tune its system parameters to meet the application-specific energy-accuracy demands.
- Our robust and extensive performance evaluation under diverse experimental settings reveal that FEEL can provide an accuracy of up to 6.94 cm with a mean latency of 3.15 ms. Further, we show that ASA yields up to 20% reduction in energy consumption.

II. Related Work

In this section, we will discuss the recent works for providing a general view of the state of the art in localization.

Vision-based localization: They rely on at least one vision sensor, such as LiDAR and camera, for localization. Zhen et al. employed LiDAR and UWB for localization in a tunnel-like environment based on Error State Kalman Filter (ESKF) [4]. Song et al. employed LiDAR and RGB depth camera for localization using visual tracking and depth information [5]. Wan et al. designed a robust localization method through fusion of LiDAR, GNSS, and IMU [6].

Non-vision based localization: Several localization methods using only non-vision based sensors, such as IMU, UWB, magnetometer, GNSS, and odometry, have also been extensively investigated. Hellmers et al. explored the combination of IMU and magnetometer [7]. While the works in [8]–[10] performed a fusion between IMU and UWB, Dobrev et al. fused radar, ultrasound (US), and odometry information [11]. Haong et al. explored the localization potential of GNSS, infrared, and UWB [12], and Zhou et al. developed a localization method using WiFi infrastructure [13].

In general, vision-based sensors have shown the potential to yield a localization accuracy of sub-10 cm, however, they are both expensive both energy- and cost-wise. As an example,a LiDAR sensor costs a few thousand USD. On the other hand, non-vision based sensors are generally cheap and consume low energy, albeit their localization accuracy is considerably lower.

III. *FEEL*: Design and Implementation

In this section, we describe the design and implementation details of our proposed localization system. We begin by providing the hardware details of our AIV design (Section III-A), then move to the software design where we present the EKF employed in our testbed (Section III-B) and the proposed ASA technique (Section III-C).

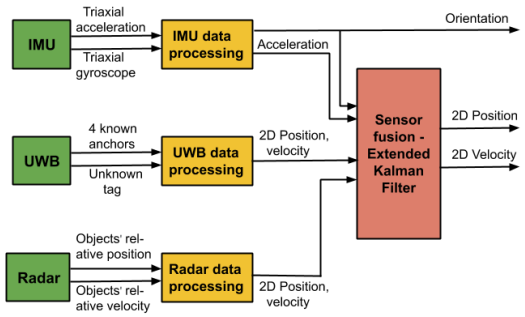

Fig. 2: Block diagram representation of FEEL showing the sensor fusion of IMU, UWB, and radar.

A. Hardware Testbed

The appropriate choice of sensors plays a vital role in determining the accuracy, latency, energy-efficiency, and cost of localization system. In this work, we explore the combination of three cost-effective and low-energy sensors: IMU, UWB, and radar. To the best of our knowledge, ours is the first attempt to explore localization using fusion of these three sensors.

IMU: In order to capture the acceleration and orientation of the AIV, we employ MPU6050 [14]. It offers a maximum sensing rate of 1 kHz and has an average power consumption of 12.89 mW.

UWB: We use four UWB anchors placed at pre-defined locations in the test environment to obtain 2D position and velocity vectors of the UWB tag placed on the AIV. For our testbed, we use Decawave DWM1001dev [15] with a maximum sensing rate of 10 Hz and an average power consumption of 0.67 W.

Radar: We employ radar for its ability to compensate for the erroneous measurements from UWB, and to detect objects in the proximity of AIV. For our testbed, we used AWR1843, which offers a maximum sensing rate of 130 Hz and has an average power consumption of 1.92 W.

The sensor fusion using EKF and other data processing steps are performed using NUCLEO-L4R5ZI processor board [16]. It has an ARM Cortex M4 32-bit microcontroller with an operating frequency of 120 MHz. The 5 V DC motors for driving the wheels are powered using a Lipo 2S battery with a capacity 3000 mAh.

B. Sensor Fusion

In this work, we use Extended Kalman Filter (EKF) as the sensor fusion technique. For simplicity in implementation, we take measurements from all three sensors as inputs for predicting position and velocity of AIV, whereas the orientation of AIV is solely determined by orientation measurement of IMU. This is depicted in Figure 2. We now provide a detailed description of the different steps of EKF involved in the design of FEEL.

Prediction: Let (a_x, a_y) denote the 2D acceleration measured by IMU and θ denote IMU orientation with respect to the initial position of AIV. Let (x, y) and (v_x, v_y) be the state variables of EKF denoting 2D position and velocity of AIV, respectively. Denoting the state variables as $X = [x \ \ y \ \ v_x \ \ v_y]^T$, their prediction $\hat{X}$ at time step k is then expressed as,

$$\hat{X_k} = FX_{k-1} + Bu_k + w_k,$$

where

$$F = \begin{bmatrix} 1 & 0 & \Delta t & 0 \\ 0 & 1 & 0 & \Delta t \\ 0 & 0 & 1 & 0 \\ 0 & 0 & 0 & 1 \end{bmatrix}, B = \begin{bmatrix} \frac{1}{2}\Delta t^2 & 0 & 0 & 0 \\ 0 & \frac{1}{2}\Delta t^2 & 0 & 0 \\ 0 & 0 & \Delta t & 0 \\ 0 & 0 & 0 & \Delta t \end{bmatrix},$$

$u_k = [a_x^k \ \ a_y^k \ \ a^k \sin\theta^k \ \ a^k \cos\theta^k]^T$ is the control input, and a is the magnitude of acceleration. Here, F and B denote the state transition matrix and control matrix, respectively, Δt is the time between successive measurements of IMU and $w_k \sim N(0, Q)$ denotes the measurement noise of IMU. Note that to indicate the time step k, we use subscripts for matrices and superscripts for state variables. The noise covariance of prediction is given by

$$\hat{P_k} = FP_{k-1}F^T + Q,$$

where Q is the noise covariance of u expressed as

$$Q = \begin{bmatrix} \sigma_{a_x}^2 & 0 & 0 & 0 \\ 0 & \sigma_{a_y}^2 & 0 & 0 \\ 0 & 0 & \sigma_{sin\theta}^2 & 0 \\ 0 & 0 & 0 & \sigma_{cos\theta}^2 \end{bmatrix}$$

Measurement: This step relies on the position and velocity measurements from UWB and radar. Due to the dependence on the measurements from two different sensors, we employ a weighted averaging to determine the effective measurement. The measurement matrix Z_k is given as

$$Z_k = \begin{bmatrix} \bar{x}^k \\ \bar{y}^k \\ \bar{v}_x^k \\ \bar{v}_y^k \end{bmatrix} + n_k = \begin{bmatrix} x_u^k \alpha_x + x_r^k (1-\alpha_x) \\ y_u^k \alpha_y + y_r^k (1-\alpha_y) \\ v_{x(u)}^k \beta_x + v_{x(r)}^k (1-\beta_x) \\ v_{y(u)}^k \beta_y + v_{y(r)}^k (1-\beta_y) \end{bmatrix} + n_k,$$

where (x_u, y_u) and $(v_{x(u)}, v_{y(u)})$ are the 2D position and velocity measurements of UWB, respectively. Similarly, (x_r, y_r) and $(v_{x(r)}, v_{y(r)})$ are the 2D position and velocity measurements of radar, respectively. α_x and α_y denote weights assigned to the position measurements of UWB along x and y-axis, respectively. Similarly, β_x and β_y denote weights assigned to the velocity measurements of UWB along x and y-axis, respectively. The weighted average of the sensor measurements is denoted with the overline character. Since the weighted average is used as state variables in the measurement model, H (the Jacobian of Z), is an identity matrix, i.e. $H = I$. The measurement noise $n_k \sim N(0, R)$, where

$$R = \begin{bmatrix} \sigma_{\bar{x}}^2 & 0 & 0 & 0 \\ 0 & \sigma_{\bar{y}}^2 & 0 & 0 \\ 0 & 0 & \sigma_{\bar{v}_x}^2 & 0 \\ 0 & 0 & 0 & \sigma_{\bar{v}_y}^2 \end{bmatrix}.$$

Here $\sigma_{\bar{x}}^2 = \alpha_x \sigma_{x_u}^2 + (1-\alpha_x)\sigma_{x_r}^2$, $\sigma_{\bar{y}}^2 = \alpha_y \sigma_{y_u}^2 + (1-\alpha_y)\sigma_{y_r}^2$, $\sigma_{\bar{v}_x}^2 = \beta_x \sigma_{v_{x(u)}}^2 + (1-\beta_x)\sigma_{v_{x(r)}}^2$, and $\sigma_{\bar{v}_y}^2 = \beta_y \sigma_{v_{y(u)}}^2 + (1-\beta_y)\sigma_{v_{y(r)}}^2$.

Update: After the sensor measurements are available, the EKF applies the correction step to the predicted values as per the following equations. The innovation matrix Y, its covariance S, and Kalman gain K are given by the following equations.

$$Y_k = Z_k - \hat{X_k}, \ \ S_k = \hat{P_k} + R, \ \ K_k = \hat{P_k} S_k^{-1}$$

Finally, the prediction and its covariance matrices are updated as

$$X_k = \hat{X_k} + K_k Y_k, \ \ P_k = (I - K_k)\hat{P_k}.$$

Due to the need of accurate localization as well as reducing the computational demands of FEEL, we run EKF in synchronization with IMU at 1 kHz. This means that UWB and radar measurement samples that are generated between two successive IMU measurements are buffered until the succeeding IMU sample is generated.

Having presented the hardware and software design of our AIV testbed, we now present the design of Adaptive Sensing Algorithm (ASA) for improving the energy-efficiency of FEEL.

C. Adaptive Sensing Algorithm (ASA)

As mentioned in Section III-A, the power consumption of sensors used in FEEL is substantially lower than LiDAR-based localization systems. However, as a good engineering practice, it is important that the AIV be designed to utilize only as much power as required to meet the demands of any given application. This improves the energy performance of AIV and significantly contributes towards development of eco-friendly industries. This motivates us to design *Adaptive Sensing Algorithm* (ASA) for opportunistically sensing information depending on the nature of AIV trajectory and the physical environment. The idea behind ASA is to dynamically adjust the sampling rate of sensors in real-time for optimizing the energy consumption and localization error of FEEL.

As already discussed in Section III-A, the energy consumption of IMU is significantly lower than UWB and radar. Hence, in ASA we keep the IMU sampling rate fixed at its maximum (1 kHz) while adapting only the sampling rates of UWB (f_u) and radar (f_r). Naturally, the energy consumption (localization error) monotonically increases (decreases) with the sensing rates, although characterizing the exact relationship between them is non-trivial and out of the scope of this work. For simplicity, we define *threshold frequencies* γ_u and γ_r as the minimum f_u and f_r, respectively, such that there is negligible reduction in accuracy ($<$1 cm in our case) compared to the best accuracy which is achieved at maximum sampling rates of sensors. Let us denote the permissible minimum and maximum frequency of UWB as $f_{u(min)}$ and $f_{u(max)}$, respectively, and those of radar as $f_{r(min)}$ and $f_{r(max)}$, respectively. Note that $f_{u(min)} < \gamma_u < f_{u(max)}$ and $f_{r(min)} < \gamma_r < f_{r(max)}$.

ASA works by increasing the sampling frequency in the following scenarios:

Algorithm 1: Adaptive Sensing Algorithm

/* For radar and UWB, add/prefix subscript r and u, respectively, to $f, f_{(min)}, f_{(max)}, \gamma, m, c$ */

Result: Determine f based on $\delta\theta$ and d

Set $m_u = 1, m_r = 0.5, c_u = -1, c_r = 0$
Initialize: $f = f_{max}$
if $\delta\theta < \theta'$ **then**
  if $f_{(min)} < f \leq \gamma$ **then**
    $f \leftarrow mf + c$
  else if $f = f_{(max)}$ **then**
    $f \leftarrow \gamma$
else
  if $f_{(min)} \leq f < \gamma$ **then**
    $f \leftarrow \gamma$
  else
    $f \leftarrow f_{max}$
  end
end
if $d < d'$ **then**
  $f_r \leftarrow f_{r(max)}$
Wait for time T and go back to Step 3

1) Change in AIV orientation: Let $\delta\theta$ denote the change in θ per T time units and θ' is the orientation threshold used by ASA. If $\delta\theta > \theta'$, then the measurements of both UWB and radar are heavily impacted. In this case, both f_u and f_r are increased aggressively to minimize the localization error. The frequency is increased as follows: If $f_r = \gamma_r$, then $f_r \leftarrow f_{r(max)}$, and if $f_{r(min)} \leq f_r < \gamma_r$, then $f_r \leftarrow \gamma_r$. Adaptation of f_u also happens in a similar fashion.
2) External objects in AIV's proximity: If an external object is in close proximity of AIV then only localization of radar is impacted. Hence, if $d \leq d'$, then $f_r \leftarrow f_{r(max)}$. Here d denotes the distance between AIV and the closest object as measured by radar and d' is the distance threshold used by ASA.

If none of the above scenarios occur, then localization accuracy can be traded off slightly for obtaining energy saving. To achieve this, ASA prudently reduces f_u and f_r until $f_{u(min)}$ and $f_{r(min)}$ are reached, respectively. Due to the heterogeneous ranges of sampling frequencies, i.e. $f_u \in [1, 10]$ Hz and $f_r \in [1, 130]$ Hz, we choose to reduce f_u linearly and f_r multiplicatively. The working of ASA is presented in Algorithm 1.

The efficacy of ASA lies in the fact that the user can configure its parameters to obtain the desired application-specific energy-accuracy performance from FEEL.

IV. Performance Evaluation

We now move to comprehensive performance evaluation of FEEL where we first describe the experimental setup (Section IV-A) and then shed light on our important findings (Section IV-B).

A. Experimental Setup

In order to conduct robust performance evaluation under a wide variety of operating conditions, we consider several profiles of indoor test environment, track, and AIV speed.

Environment profile: We evaluate FEEL in three test environments with different physical characteristics as shown in Figure 3.

E_1: In this environment, shown in Figure 3a, a couple of large objects are located around the track. E_1 enables us to understand the performance of FEEL in a typical office environment with sparse distribution of objects.

E_2: In this environment, shown in Figure 3b, there are several objects, such as chairs, tables, and a few plants, located in close proximity to the track. E_2 helps us to assess the performance of FEEL in a typical factory/warehouse environment with dense distribution of objects.

E_3: This is a narrow, long corridor with no other apart from AIV as shown in Figure 3c. E_3 enables us to understand the performance of FEEL in narrow spaces such as tunnels with extremely low margin of error and strong radio wave reflections off the walls.

Track profiles: In our investigation, we consider two track profiles: *straight track* and *race track*. As the names suggests, while in straight track profile the AIV drives along a straight line between two pre-defined points, in race track profile, the AIV trajectory resembles an oval shape.

Speed profiles: Experimenting with different speed profiles helps us identify the speed limits under which FEEL provides necessary performance guarantees. Since the maximum permissible speed of our AIV is $4\,\mathrm{kmph}$, we consider two speed profiles: low ($1.2\,\mathrm{kmph}$) and high ($4\,\mathrm{kmph}$).

As mentioned in Section III-B, EKF runs at $1\,\mathrm{kHz}$ implying that Δt=$1\,\mathrm{ms}$. In order to compute Q and R, we record sensor measurements by running several tests under different experimental conditions described above. By comparing the recorded values against ground truth, we deduce $[\sigma^2_{a_x}, \sigma^2_{a_y}, \sigma^2_{\sin\theta}, \sigma^2_{\cos\theta}]$=[2.31, 0.60, 0.32, 0.65]$\times 10^{-3}$. By empirically setting α_x=α_y=0.7 and β_x=β_y=0.4, we obtain $[\sigma^2_{\bar{x}}, \sigma^2_{\bar{y}}, \sigma^2_{\bar{v}_x}, \sigma^2_{\bar{v}_y}]$=[0.14,0.06, 0.13,0.11]. As concerns the parameters of ASA, we empirically set θ'=10°, d'=$1\,\mathrm{m}$, and T=$1\,\mathrm{s}$. These parameters can be tuned based on the expected application-specific requirements. Additionally, $f_{u(max)}$=$10\,\mathrm{Hz}$ and $f_{r(max)}$=$130\,\mathrm{Hz}$. Other parameter configurations, such as $f_{u(min)}, f_{r(min)}, \gamma_u$, and γ_r, will be discussed in the next section.

B. Experimental Results

We begin by presenting the localization accuracy and latency performance of FEEL. Note that although we conduct performance evaluation across several profiles explained earlier, due to space constraints we present only the most interesting findings in this paper.

Figure 4a shows a head-to-head comparison of localization accuracy of FEEL against two commonly used non-vision based localization techniques: IMU-radar and IMU-UWB. In

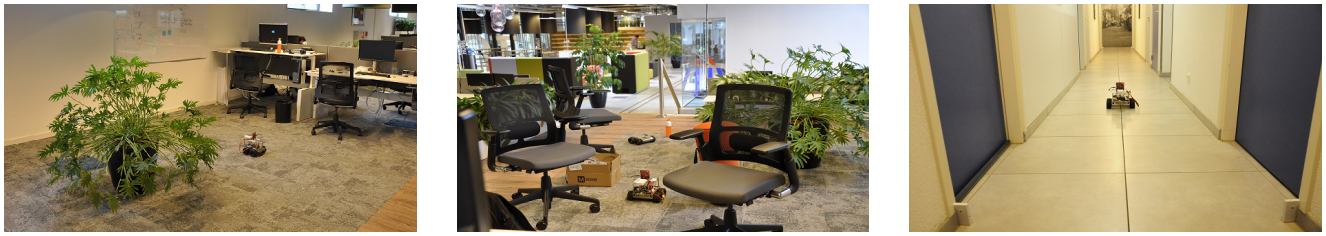

(a) (b) (c)

Fig. 3: Indoor test environments used for performance evaluation of FEEL. a) E_1: office environment with sparsely distributed objects, b) E_2: office environment with densely distributed objects, and c) E_3: narrow, long corridor with no other objects.

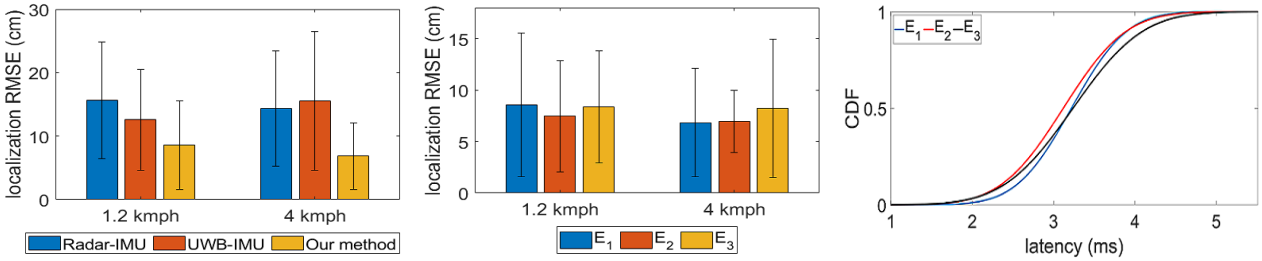

(a) (b) (c)

Fig. 4: Performance evaluation of FEEL. (a) Comparison of localization RMSE with two common localization methods, (b) Localization RMSE in three test environments (c) Localization latency in three environments and high speed profile.

order to obtain a fair and consistent performance analysis, we implemented these localization techniques on our testbed. The presented findings correspond to the two speed profiles in E_1 and straight track. It can be seen that FEEL outperforms others giving RMSE of $8.57\,\mathrm{cm}$ and $6.85\,\mathrm{cm}$ for low and high speed profiles, respectively. FEEL yields a significant accuracy improvement of up to 2x and 2.2x over IMU-radar and IMU-UWB methods, respectively. Interestingly, the accuracy of our method increases with the AIV speed. This behavior is attributed to the higher localization accuracy of the radar module used in our testbed.

We present the localization accuracy of FEEL in the three test environments for straight track and both speed profiles in Figure 4b. It can be seen that in all cases, the RMSE is sub-$9\,\mathrm{cm}$. Interestingly, for low speed profile, the performance in E_2 better than in E_1 and E_3. The rationale behind this behavior is that the large number of objects present in E_2 aid the radar in localizing the AIV better. We observe comparable performance of FEEL in case of race track profile also.

We now move to measuring the localization latency of FEEL. Figure 4c presents our findings for straight track in the three test environments. It can be observed that the mean latency is $3.15\,\mathrm{ms}$. The extremely low latency profile demonstrates the potential of the usage of FEEL in ultra-low latency applications. Further, the similar latency measurements in all test environments also demonstrate robustness of FEEL's latency performance to the characteristics of the operating environment.

We now compare the performance of FEEL (without ASA) with state of the art in localization. Note that the power consumption presented is for the overall system including the sensors. As can be seen from Table II, only UWB-LiDAR [17] matches the accuracy and latency provided by FEEL, however this comes at the expense of high power consumption and overall system cost since it employs LiDAR. The missing details of [9] is due to the insufficient details provided in the article. To summarize, FEEL outperforms the state of the art

	IMU-UWB [9]	UWB-LiDAR [17]	IMU-UWB-LiDAR [4]	Radar-US [11]	IMU-UWB -Radar (FEEL)
Test speed (kmph)	2.5	2.88	2.52	4.32	4
Max. accuracy (cm)	10.2	7.6	10	15	6.94
Mean latency (ms)	–	3	–	–	3.15
Power consp. (W)	–	>10	>10	∼6.06	4.19
System cost ($)	–	>4500	>4500	>4000	∼400

TABLE I: System- and performance-level comparison of FEEL with state of the art in localization.

	IMU-UWB [1]	UWB-LiDAR [2]	IMU-UWB-LiDAR [3]	Radar-US [4]	IMU-UWB -Radar (Ours)
Test speed (kmph)	2.5	2.88	2.52	4.32	4
Max. accuracy (cm)	10.2	7.6	10	15	6.94
Mean latency (ms)	–	3	–	–	3.15
Power consp. (W)	–	>10	>10	∼6.06	4.19
System cost ($)	–	>4500	>4500	>4000	∼400

TABLE II: System- and performance-level comparison of FEEL with state of the art in localization.

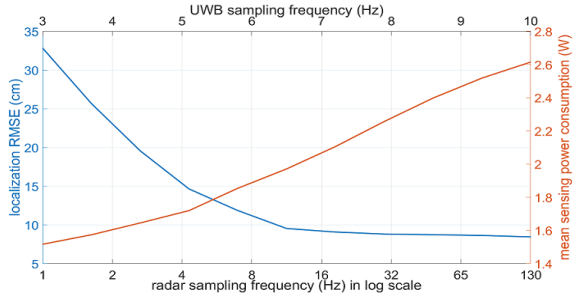

Fig. 5: Trade off between localization error and sensing power consumption over a wide range of f_r and f_u in E_2.

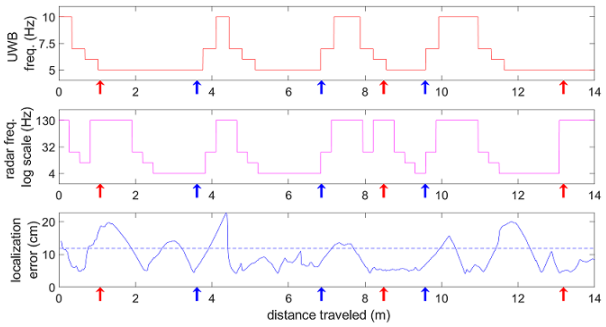

Fig. 6: Demonstration of sampling frequency adaptation of ASA and the resulting localization error in response to turns (blue arrows) and objects (red arrows) in the environment.

in localization comprehensively.

Finally, we now move to the energy-efficiency aspect of FEEL. Before moving to assessing the performance of the proposed ASA, it is important to understand the influence of f_r and f_u on localization accuracy and power consumption in order to determine $f_{r(min)}, f_{u(min)}, \gamma_r$ and γ_u. Figure 5 presents these dynamics for E_2 and race track profile. It can be seen that while the localization error falls off exponentially with increasing f_r and f_u, the sensing power consumption increases linearly on a log scale for f_r and a linear scale for f_u. Interestingly, radar information has significant redundancy that can be exploited to achieve energy efficiency in ASA. It is worth mentioning that the variation looks similar for other experimental profiles also. From Figure 5, it is clear that γ_r=16 Hz and γ_r=7 Hz. It can be seen that at these values, there is approximately 18% reduction in energy consumption in comparison with that at the maximum sensing rates. This demonstrates the scope of improving the energy efficiency of FEEL with negligible compromise on accuracy.

With the above values for frequency parameters, we now present the performance evaluation of ASA in E_1 on race track. The total length of the track is $14\,\mathrm{m}$ with three large objects around the track. The three objects and turns are marked in Figure 6 using red and blue arrows, respectively. As can be seen, sensing rate increase as a response to objects starts prior to reaching the object due to the radar detecting them, whereas response to turns starts only once the AIV starts changing its trajectory. Our measurements reveal that due to the sampling rate adaptation of ASA, there is approximately 20% reduction in power consumption of AIV, although the localization RMSE is measured to be $12\,\mathrm{cm}$.

V. Conclusions

Autonomous indoor vehicles will be heavily employed in automation industries/warehouses in the near future. These AIVs require high localization accuracy at ultra-low latency and low-energy demands. In this paper, we proposed a system called *FEEL* for indoor localization by fusing IMU, UWB, and radar. We presented the design of the custom-built hardware for showing the proof of concept. In order to address the energy challenges, we proposed *Adaptive Sensing Algorithm (ASA)* for opportunistically tuning the sampling frequency to minimize energy consumption by trading off marginally for accuracy. We performed extensive evaluation and found that the localization accuracy of FEEL is within $7\,\mathrm{cm}$ while the mean localization latency is around $3.15\,\mathrm{ms}$. We showed that ASA provides a considerable improvement in the energy performance of FEEL of up to 20%. Further, we showed that FEEL comprehensively outperforms state of the art in indoor localization. We believe that the work presented here will become one of the benchmarks for further research in this domain.

References

[1] O. Holland, E. Steinbach, R. V. Prasad, Q. Liu, Z. Dawy, A. Aijaz, N. Pappas, K. Chandra, V. S. Rao, S. Oteafy *et al.*, "The ieee 1918.1 "tactile internet" standards working group and its standards," *Proceedings of the IEEE*, vol. 107, pp. 256–279, 2019.

[2] J. A. Cocoma-Ortega and J. Martínez-Carranza, "Towards high-speed localisation for autonomous drone racing," in *Mexican International Conference on Artificial Intelligence*. Springer, 2019.

[3] N. Zhu, J. Marais, D. Betaille, and M. Berbineau, "Gnss position integrity in urban environments: A review of literature," *IEEE Transactions on Intelligent Transportation Systems*, vol. 19, pp. 2762 – 2778, 2018.

[4] W. Zhen and S. Scherer, "Estimating the localizability in tunnel-like environments using lidar and uwb," in *2019 International Conference on Robotics and Automation (ICRA)*. IEEE, 2019, pp. 4903–4908.

[5] H. Song, W. Choi, and H. Kim, "Robust vision-based relative-localization approach using an rgb-depth camera and lidar sensor fusion," *IEEE Transactions on Industrial Electronics*, vol. 63, pp. 3725–3736, 2016.

[6] G. Wan, X. Yang, R. Cai, H. Li, Y. Zhou, H. Wang, and S. Song, "Robust and precise vehicle localization based on multi-sensor fusion in diverse city scenes," in *IEEE International Conference on Robotics and Automation (ICRA)*, 2018.

[7] H. Hellmers, Z. Kasmi, A. Norrdine, and A. Eichhorn, "Accurate 3d positioning for a mobile platform in non-line-of-sight scenarios based on imu/magnetometer sensor fusion," *Sensors*, vol. 18, no. 1, 2018.

[8] L. Yao, Y.-W. A. Wu, L. Yao, and Z. Z. Liao, "An integrated imu and uwb sensor based indoor positioning system," in *International Conference on Indoor Positioning and Indoor Navigation (IPIN)*. IEEE, 2017.

[9] A. Marquez, B. Tank, S. K. Meghani, S. Ahmed, and K. Tepe, "Accurate uwb and imu based indoor localization for autonomous robots," in *IEEE Canadian Conference on Electrical and Computer Engineering*, 2017.

[10] D. Feng, C. Wang, C. He, Y. Zhuang, and X.-G. Xia, "Kalman-filter-based integration of imu and uwb for high-accuracy indoor positioning and navigation," *IEEE Internet of Things Journal*, vol. 7, pp. 3133–3146, 2020.

[11] Y. Dobrev, S. Flores, and M. Vossiek, "Multi-modal sensor fusion for indoor mobile robot pose estimation," in *IEEE/ION Position, Location and Navigation Symposium*, 2016.

[12] G.-M. Hoang, B. Denis, J. Härri, and D. T. Slock, "Robust and low complexity bayesian data fusion for hybrid cooperative vehicular localization," in *IEEE International Conference on Communications (ICC)*, 2017.
[13] M. Zhou, H. Yuan, Y. Wang, W. Tan, and Z. Tian, "Indoor uav localization using manifold alignment with mobile ap detection," in *IEEE International Conference on Communications (ICC)*, 2019.
[14] InvenSense Inc, "MPU-6000 and MPU-6050 Register Map and Descriptions Revision 4.2," 2013.
[15] Decawave, "Product Datasheet: DWM1001-DEV," 2017.
[16] STMicrocontrollers, "STM32 Nucleo-144 boards User Manual," 2019.
[17] Y. Song, M. Guan, W. P. Tay, C. L. Law, and C. Wen, "Uwb/lidar fusion for cooperative range-only slam," in *IEEE International Conference on Robotics and Automation (ICRA)*, 2019.